HHS Public Access

Author manuscript

Cancer Res. Author manuscript; available in PMC 2018 August 15.

Published in final edited form as:

Cancer Res. 2017 August 15; 77(16): 4486–4497. doi:10.1158/0008-5472.CAN-16-2643.

NF1$^{+/-}$ hematopoietic cells accelerate malignant peripheral nerve sheath tumor development without altering chemotherapy response

Rebecca D. Dodd[a,g], **Chang-Lung Lee**[a], **Tess Overton**[a], **Wesley Huang**[a], **William C. Eward**[b], **Lixia Luo**[a], **Yan Ma**[a], **Davis R. Ingram**[c], **Keila E. Torres**[d], **Diana M. Cardona**[e], **Alexander J. Lazar**[c], and **David G. Kirsch**[a,f]

[a]Department of Radiation Oncology, Duke University Medical Center, Durham, North Carolina, 27708

[b]Department of Orthopaedic Surgery, Duke University, Durham, North Carolina, 27708

[c]Department of Pathology, The University of Texas MD Anderson Cancer Center, Houston, TX, USA

[d]Department of Surgical Oncology, The University of Texas MD Anderson Cancer Center, Houston, TX, USA

[e]Department of Pathology, Duke University, Durham, North Carolina, 27708

[f]Department of Pharmacology and Cancer Biology, Duke University Medical Center, Durham, North Carolina, 27708

Abstract

Haploinsufficiency in the tumor suppressor NF1 contributes to the pathobiology of type 1 neurofibromatosis, but a related role has not been established in malignant peripheral nerve sheath tumors (MPNST) where NF1 mutations also occur. Patients with NF1-associated MPNST appear to have worse outcomes than patients with sporadic MPNST, but the mechanism underlying this correlation is not understood. To define the impact of stromal genetics on the biology of this malignancy, we developed unique mouse models that reflect the genetics of patient-associated MPNST. Specifically, we used adenovirus-cre injections to generate MPNST in Nf1$^{Flox/Flox}$; Ink4a/Arf$^{Flox/Flox}$ and Nf1$^{Flox/-}$; Ink4a/Arf$^{Flox/Flox}$ paired littermate mice to model tumors from NF1-wildtype and NF1-associated patients, respectively. In these models, Nf1 haploinsufficiency in hematopoietic cells accelerated tumor onset and increased levels of tumor-infiltrating immune cells comprised of CD11b+ cells, monocytes and mast cells. We observed that mast cells were also enriched in human NF1-associated MPNST. In a co-clinical trial to examine how the tumor microenvironment influences the response to multi-agent chemotherapy, we found that stromal Nf1 status had no effect. Taken together, our results clarify the role of the NF1-haploinsufficient tumor microenvironment in MPNST.

Corresponding author. David G. Kirsch, Duke University Medical Center, DUMC Box 91006, Durham, North Carolina 27708, Tel: 919-681-8605, david.kirsch@duke.edu.

[g]Present address: Department of Internal Medicine, University of Iowa, Iowa City, Iowa 52242

The authors have no conflicts of interest to disclose.

Keywords

MPNST; NF1; sarcoma; tumor microenvironment; mast cell

Introduction

Soft tissue sarcomas (STS) are tumors of the connective tissue comprised of a diverse array of subtypes. Frequent disruptions in the Ras pathway are a hallmark of many STS (1, 2). Although mutations in *Ras* itself have been frequently identified in rhabdomyosarcomas in children (3–5), mutations in other Ras pathway gene members are more common in many adult soft tissue sarcomas, including the tumor suppressor neurofibromin (*NF1*), a negative regulator of Ras protein function (6). Loss-of-function mutations in *NF1* have also been identified in a wide spectrum of other sporadic tumors, including lung adenocarcinoma, glioblastoma, melanoma, and breast cancer (7). Additionally, neurofibromin plays a central role in the cancer predisposition syndrome Neurofibromatosis Type I (also abbreviated NF1), a common genetic condition that affects 1 in 3,000 children. Patients with Neurofibromatosis type I (NF1) have germline loss of a single *NF1* allele, resulting in *NF1* haploinsufficiency (*NF1* +/−) and hyperactive Ras signaling in all cells throughout the body. Loss of the second *NF1* allele results in the formation of neurofibromas, benign growths arising from nerves, which occur in >95% of NF1 patients. Neurofibromas can result in severe morbidity, causing disfiguration, pain, and occasionally lethality. Importantly, neurofibromas occur predominantly in Neurofibromatosis patients, suggesting that *NF1* haploinsufficiency plays a role in neurofibroma development, although sporadic neurofibromas do develop in the absence of *NF1* haploinsufficiency. Mouse models have demonstrated that *Nf1* haploinsufficient supporting stromal cells (endothelial cells, immune cells, fibroblasts, etc) can accelerate the development and vascularization of neurofibromas (8, 9), although *Nf1* haploinsufficient stroma is not a requirement for neurofibroma formation in mice (10, 11). Neurofibromatosis patients are also at increased risk for developing soft-tissue sarcomas, most commonly malignant peripheral nerve sheath tumors (MPNSTs), with a 5-year survival of less than 50% (12, 13). However, unlike neurofibromas, the role of the *NF1* haploinsufficient tumor microenvironment in MPNST biology is not well understood, as MPNSTs also occur in non-NF1 patients (referred to as sporadic MPNSTs).

MPNSTs present with two distinct clinical histories: NF1-associated (in Neurofibromatosis patients) and sporadic (in the general, non-NF1 population). Approximately 8–13% of Neurofibromatosis patients will develop MPNSTs in their lifetime, with a mean age of 26 years at diagnosis. In contrast, sporadic MPNSTs have a much lower incidence (<0.1%), with an average age onset of 62 years (14). NF1-associated and sporadic MPNSTs are indistinguishable by gene expression profile, anatomical location, and histopathology, although groups have reported differing levels of p53 staining between the two tumor types (15). However, outcomes for NF1-associated MPSNTs appear worse (12, 16), although survival may be improving (13, 17). Additionally, NF1-assoicated MPNSTs may respond less favorably to cytotoxic chemotherapy, including a standard doxorubicin/ifosfamide combination used for many sarcoma patients (18). It is unknown if the disparity in outcome

is due to clinical factors—such as Neurofibromatosis patients presenting later with MPNST due to the challenge of identifying the sarcoma within a patient with multiple large neurofibromas—or if the disparity in outcome is due to intrinsic biological properties of the tumors, such as worse response to chemotherapy (19). A better understanding of the biological differences driven by the MPNST microenvironment in NF1 patients might have important clinical implications that could impact patient care and reveal new cellular targets for MPNST-directed therapy.

To address this question experimentally, we have developed a new mouse model of malignant peripheral nerve sheath tumor (MPNST) to explore the role of *NF1* haploinsufficiency in tumor biology. Previously, we used Cre-loxP technology to generate the first mouse model of temporally and spatially restricted MPNST in $Nf1^{Flox/Flox}$; $Ink4a/Arf^{Flox/Flox}$ mice (20) and established an accessible preclinical platform for testing novel therapies. With this approach MPNSTs develop in $Nf1^{Flox/Flox}$; $Ink4a/Arf^{Flox/Flox}$ mice following injection of an adenovirus expressing Cre recombinase (Ad-Cre) into the sciatic nerve. Cre deletes both *Nf1* and the commonly mutated tumor suppressor *Ink4a/Arf* (known as p16/19 in mice and *CDKN2A* or p14/p19 in humans) in cells of the surrounding nerve sheath. The tumor microenvironment remains wild type for both *Nf1* and *Ink4a/Arf*, as the conditional floxed alleles are not deleted in the stroma. These tumors faithfully reflect the human MPNST by histology and immunohistochemistry. Additionally, these tumors have mutant *Cdkn2a* and wild-type *p53*, a genetic combination found in the majority of sporadic and NF1-associated of MPNSTs (21, 22). We have used this system to characterize the biological properties of *Nf1*-deleted sarcoma and as a platform to test MEK inhibitors *in vivo* (20). To model the unique genetics of NF1-associated MPNSTs, here we developed a complementary model in $Nf1^{Flox/-}$; $Ink4a/Arf^{Flox/Flox}$ mice. Upon Ad-Cre injection, this model generates MPNSTs deleted for both *Nf1* and *Ink4a/Arf* with a surrounding tumor microenvironment comprised of $Nf1^{Flox/-}$ cells, mimicking *NF1* haploinsufficiency (ie: $NF1^{+/-}$) found in Neurofibromatosis patients through the loss of a single *Nf1* allele. In this study, we compared the two models of MPNST with either *Nf1* intact or *Nf1* haploinsufficient stroma to investigate the role of the *NF1* haploinsufficient tumor microenvironment in MPNST biology.

Materials and Methods

Mouse sarcoma model

All mouse work was conducted in accordance with Duke University Institutional Animal Care and Use Committee approved protocols. The $Nf1^{Flox/Flox}$ and $Nf1^{+/-}$ mice (23, 24) were obtained from Jackson laboratories, and $Ink4a/Arf^{F/F}$ mice (25) were provided by Ron Dephino. Tumors were generated by injection of Ad-Cre (University of Iowa, Iowa City, IA; Vector core) into the sciatic nerve of $Nf1^{Flox/Flox}$; $Ink4a/Arf^{Flox/Flox}$ or $Nf1^{Flox/-}$; $Ink4a/Arf^{Flox/Flox}$ compound mutant mice as previously described (20). Briefly, the nerve was exposed by an incision in the surrounding muscle of the upper left flank, followed by injection of 25 μL Ad-Cre mixed with calcium phosphate into the nerve (26).

Histology, immunostaining, and quantification

Antibodies for immunohistochemistry were used at 1:200 and include: S100 protein (DakoCytomation), pERK (Cell Signaling Technology, clone D13.14.4E), pS6 (Cell Signaling Technology, clone D68F8), Ki67 (BD Pharmagen, clone B56), cleaved caspase 3 (BD Pharmagen, clone CPP32), and KIT (DakoCytomation). All immunostaining was conducted with citrate-based antigen retrieval. The following stains were performed by the Duke Research Histology Lab: CD31, SMA, CD45, CD3, B220, CD11C, CD68, and Iba1. To visualize mast cells, slides were stained with toluidine blue solution (0.02% toluidine blue in 1% NaCl, pH 2.2) for 2 minutes, followed by two washes in distilled water and three washes in 100% ethanol. Quantification of cells staining for an antibody or toluidine blue was performed on 6 fields of a single slide to generate the total number of positively stained cells. 20× fields were used for all analyses except for Ki67 levels, which used 40× fields.

Cell Doubling Assay

The MPNST mouse cell lines were derived from primary MPNSTs in $Nf1^{Flox/Flox}$; $Ink4a/Arf^{Flox/Flox}$ or $Nf1^{Flox/-}$; $Ink4a/Arf^{Flox/Flox}$ mice in our own laboratory. These cells were authenticated by PCR genotyping (18) within the last 6 months. Doublings of cell populations has been reported previously (27). Three independent cell lines of each genotype were seeded at 10,000 cells per well for 48 hours, and the number of cell doublings was calculated. From this population, another 10,000 cells were plated, and cell doublings were calculated for at least four iterations. The graph shows the average of three independent cell lines per genotype.

Bone marrow transplantation

Whole bone marrow cells (WBMs) were isolated according to methods described previously (28). WBMs from donor mice with the indicated genotype and expressing tdTomato fluorescent protein were transplanted into 8-week-old recipient mice 6 hours after two fractions of 4.75 Gy total-body irradiation (TBI) with an interval of 18 hrs. TBI was performed 50 cm from the radiation source with a dose rate of 220 cGy/min with 320 kVp X-rays, using 12.5 mA and a filter consisting of 2.5 mm Al and 0.1 mm Cu (X-RAD 320 Biological Irradiator, Precision X-ray). The dose rate was measured with an ion chamber by members of the Radiation Safety Division at Duke University. At 12 weeks after bone marrow transplantation, donor-derived engraftment of bone marrow cells in the peripheral blood was assessed by flow cytometry according to methods previously described (28).

Analyzing tumor-associated immune cells by flow cytometry

Cells were dissociated from tumors according to methods described previously (29). Total cells dissociated from tumors were blocked with rat anti-mouse CD16/32 IgG (BD Pharmingen) and then stained with FITC conjugated anti-mouse Ly-6C (clone: HK1.4), phycoerythrin (PE) conjugated anti-mouse CD11c (clone: N418), PE-Cy5 conjugated anti-mouse CD11b (clone: M1/70), APC conjugated anti-mouse NK1.1 (clone: PK136) (all from eBioscience) and APC-Cy7 conjugated anti-mouse Ly-6G (clone: 1A8) (BioLegend). All antibodies were diluted 1:400. Data were collected from at least 200,000 single cells by FACSCanto (BD Pharmingen) and analyzed by Flowjo (Tree Star, Inc). Tumor-associated

immune cells were characterized based on the expression of phenotypic markers (30). Dendritic cells: $CD11b^+$ $CD11c^+$, monocytes: $CD11b^+$ $CD11c^-$, monocytic myeloid derived suppresser cells (MDSCs): $CD11b^+$ $CD11c^-$ Ly6GLy6C^{high}, and granulocytic MDSCs: $CD11b^+$ $CD11c^-$ $Ly6G^+$ Ly6C^{low}.

Human Tissue Microarray analysis

A human MPNST tissue microarray (TMA) was built using patient samples obtained under approval of the Institutional Review Board of The University of Texas MD Anderson Cancer Center as previously described (13, 31). An anonymized, full clinical database, including the neurofibromatosis status of each patient, was constructed. KIT (DakoCytomation) immunohistochemistry was performed on TMA slides as described previously (32, 33). In short, slides were deparaffinized using Bond Dewax solution, subjected to citrate-based antigen retrieval, and visualized using a polymer-HRP secondary antibody with DAB as the chromogen and hematoxylin as the counterstain. Each pair of duplicate, 0.6 mm-diameter samples was scored by counting KIT-positive mast cells in each of the paired cores and averaged. They were then triple binned as having <5, 5–50, or >50 mast cells for analysis. Primary and recurrent disease sites were tabulated separately for each patient. When a single patient was represented by multiple tumor samples, an average value was recorded.

Quantitative RT-PCR

RNA was isolated from tumors and cells by TRIzol. cDNA synthesis was conducted with iScript (Bio-Rad). qRT-PCR was conducted on an iQ5 instrument (Bio-Rad) using the $\Delta\Delta C_t$ method.

Doxorubicin/IFO treatment and tumor growth analysis

Mice were treated with a single bolus of vehicle or Doxorubicin/IFO (15 mg/kg Doxoribicin IP and 50 mg/kg IFO via tail vein) when they reached a volume of 200–300 mm^3. Tumors were measured by calipers 3 times weekly. Tumor volumes were calculated using the formula $V = (\pi \times L \times W \times H)/6$, with L, W, and H representing the length, width, and height of the tumor in mm, respectively. Criteria for defining treatment response included both volumetric analysis and a delay in tumor growth kinetics. For waterfall plot analyses, percentage of maximal change is reported as the greatest percentage of loss in tumor volume from baseline for tumors responding to treatment, as previously reported (34). Tumors that did not respond to treatment are shown as greatest percentage of gain in tumor volume from baseline over the course of the treatment. In this presentation of the data, change in tumor volume is capped at 100%.

Statistical analysis

Graphs and statistics were conducted in GraphPad 6.0. A nonparametric Student t test was conducted to determine differences between treatment groups. Comparison of survival curves was performed using the log-rank (Mantel-Cox) test, with a p-value of less than 0.05 considered statistically significant.

Results

A new mouse model for MPNST development with *Nf1* happloinsufficient stroma

To model the unique stromal genetics of MPNSTs in distinct patient groups, we created a breeding strategy that would generate paired littermate mice with either *Nf1* haploinsufficient ($Nf1^{Flox/-}$) or wild-type *Nf1* ($Nf1^{Flox/Flox}$) stroma. By utilizing conditional alleles, we can fully delete *Nf1* and *Ink4a/Arf* in tumor cells of both models to generate *Nf1*-null, *Ink4a/Arf* –null MPNSTs, while still maintaining endogenous expression of any floxed alleles in the surrounding stroma (Figure 1A–B). Thus, injection of Ad-Cre into the sciatic nerve of $Nf1^{Flox/-}$; $Ink4a/Arf^{Flox/Flox}$ ($NI^{F/-}$) mice will generate MPNSTs that are deleted for *Nf1* and *Ink4a/Arf*, while retaining expression of *Ink4a/Arf* and a single copy of *Nf1* in the surrounding stroma, modeling *NF1* haploinsufficiency in Neurofibromatosis patients. In contrast, Ad-Cre delivery into $Nf1^{Flox/Flox}$; $Ink4a/Arf^{Flox/Flox}$ ($NI^{F/F}$) mice will generate MPSNTs that are deleted for *Nf1* and *Ink4a/Arf*, but surrounded by wild-type stroma, modeling sporadic MPNSTs in non-NF1 patients.

Nf1 haploinsufficient stroma accelerates the onset of MPNST in mice

A cohort of $NI^{F/F}$ (n=59) and $NI^{F/-}$ (n=37) paired littermate mice were injected with Ad-Cre into the sciatic nerve to generate MPNSTs. Tumors developed more rapidly in $NI^{F/-}$ mice than in $NI^{F/F}$ littermates ($p<0.05$, 101 days vs. 139 days, Figure 1C). Review of the histopathology by a sarcoma pathologist demonstrated that all tumors were MPNSTs based on spindle cell morphology and lack of myogenic staining. All tumors were histologically indistinguishable by genotype and showed similar levels of S100B and Ki67 staining (Figure 1D–E). To study cell intrinsic properties of the MPNSTs, we generated cell lines from multiple tumors across the two genotypes. The doubling rate of cells from tumors from $NI^{F/-}$ and $NI^{F/F}$ mice were indistinguishable (Figure 1F, showing the average of three independent cell lines per genotype). Taken together, these data suggest the $NI^{F/-}$ model represents the distinctly unique characteristics of NF1-associated MPNSTs, which are histologically similar to sporadic MPSNTs but develop at an earlier age.

Characterizing the *Nf1* haploinsufficient tumor microenvironment

Neurofibromin regulates signaling through the Ras-MEK-ERK and PI3K/mTOR pathways, and *NF1* haploinsufficiency can lead to elevated levels of pERK and pS6 that result in altered activity of endothelial cells, fibroblasts, and immune cells (35). Thus, we hypothesized that the tumor microenvironments of $NI^{F/F}$ and $NI^{F/-}$ MPSNTs would differ in the number or activity of these cell types. To explore these potential differences, we performed immunohistochemical analysis for levels of pERK and pS6, in addition to components of the tumor microenvironment including tumor vasculature, fibroblasts, and immune cells. Levels of pS6 and pERK were high in most MPNSTs evaluated, with no difference between stromal genotypes (Figure 2A–B). To examine endothelial cells, we quantified the number of CD31+ cells per tumor. Vascular density between the two genotypes was virtually identical (Figure 2C). Fibroblast content and activity were analyzed by SMA+ cells (a marker of fibroblast activation (36, 37)) and levels of Masson's Trichrome staining (a measure of collagen content). There was no discernable difference in either metric of fibroblast activity (Figure 2D–E). To examine immune cell infiltrate, we analyzed

CD45+ cells (Figure 2F). There was a greater than 2-fold increase in the number of CD45+ cells in $NI^{F/-}$ MPNSTs, suggesting a large immune cell infiltration from the *Nf1* haploinsufficient microenvironment.

The *Nf1* haploinsufficient hematopoietic compartment accelerates MPNST onset

We hypothesized that the increased hematopoietic infiltrate in the $NI^{F/-}$ MPNSTs might contribute to the accelerated kinetics of tumor development observed in Figure 1C. Alternatively, the $NI^{F/-}$ mice could develop MPNSTs more rapidly because tumorigenesis in the $NI^{F/-}$ mice only requires Cre to delete a single $Nf1^{Flox}$ allele (a "second hit"), in contrast to deletion of two $Nf1^{Flox}$ alleles in $NI^{F/F}$ mice. To test these hypotheses, we performed bone marrow transplants from $NI^{F/-}$ or $NI^{F/F}$ donor mice into $NI^{F/F}$ recipient animals (Figure 3A). Recipient $NI^{F/F}$ mice received whole body irradiation to eliminate the majority of *Nf1* wild-type bone marrow. Half of the mice received $NI^{F/-}$ bone marrow, while the other half received $NI^{F/F}$ bone marrow. A ubiquitous fluorescent reporter in the donor mice (membrane-bound Tomato Red, mTom) was used to assess engraftment. Four weeks after recovery, the average percentage of mTomato+ peripheral blood cells was 82.6% +/− 1.63 (Supplementary Figure 1). At this time, the mice were injected with Ad-Cre into the sciatic nerve. Similar to the results in Figure 1C, mice that received $NI^{F/-}$ bone marrow developed tumors more rapidly than mice that received $NI^{F/F}$ bone marrow (Figure 3B). Histological analysis of the tumors showed increased infiltration of hematopoietic cells in mice receiving $NI^{F/-}$ bone marrow, illustrated by CD45 staining. (Figure 3C). Both genotypes of MPNSTs had similar levels of Ki67 staining (Figure 3C). These data demonstrate that differences in efficiency of deletion of *Nf1* by Cre in the tumor-initiating cell do not fully explain the different time to tumor development between MPNSTs in $NI^{F/-}$ and $NI^{F/F}$ mice. Instead, these results indicate that factors derived from the bone marrow compartment are responsible for the accelerated tumor development in $NI^{F/-}$ mice. Thus, the *Nf1* haploinsufficient tumor microenvironment directly impacts MPNST biology.

Enrichment of myeloid cell populations in *Nf1* haploinsufficient MPNST

To further characterize the $CD45^+$ immune cell infiltrate that is associated with accelerated MPNST development in $NI^{F/-}$ mice, we used flow cytometry and immunohistochemistry to analyze the primary MPNSTs generated in Figure 1. Flow cytometry allowed us to interrogate multiple immune cell types in MPNSTs and showed an increase in $CD11b^+$ myeloid cells in tumors from $NI^{F/-}$ mice (Figure 4A–B). Within the $CD11b^+$ population, there was no difference between the two genotypes in levels of $CD11b^+$ $CD11c^+$ dendritic cells. However, the percentage of $CD11b^+$ $CD11c^-$ monocytes was significantly higher in $NI^{F/-}$ MPNSTs. Recent studies demonstrate a critical role for myeloid-derived suppressor cells (MDSCs) in promoting tumor initiation (38, 39). Therefore, we also compared the percentage of MDSCs between $NI^{F/-}$ and $NI^{F/F}$ MPNSTs, but we did not observe a significant difference in either monocytic MDSCs ($CD11b^+$ $CD11c^-$ $Ly6G^-$ $Ly6C^{high}$) or granulocytic MDSCs ($CD11b^+$ $CD11c^-$ $Ly6G^+$ $Ly6C^{low}$). Immunohistochemical analysis found no difference in T cells ($CD3^+$) or B cells ($B220^+$) (Figure 4C), supporting the flow analysis demonstrating that the major difference between the immune infiltrates was a consequence of the number of myeloid cells. IHC results further supported the flow data by confirming that $CD11c^+$ dendritic cells were not enriched in $NI^{F/-}$ MPNSTs. Notably,

although we observed an increase in $CD11b^+$ cells in $NI^{F/-}$ MPNSTs by flow cytometry, IHC staining using two macrophage markers ($CD68^+$ and $Iba1^+$) did not show a significant difference in MPNSTs of either genotype (Figure 4C).

We also used histological techniques to examine cell populations that were not captured by our flow analysis, including mast cells stained by toluidine blue. Mast cells are tissue-resident, histamine-rich, cKit+ myeloid cells that play a fundamental role in the allergic response and may influence cancer development in some cellular contexts (40). Mast cells were strongly enriched in MPNSTs from $NI^{F/-}$ mice, with high levels found exclusively in tumors from mice with an *Nf1* haploinsufficient tumor microenvironment (Figure 4C–D). Importantly, there were no differences in mast cell number between $NI^{F/F}$ and $NI^{F/-}$ mice in other tissues, including mast-cell rich skin and tongue samples (Supplemental Figure 2), suggesting their enrichment is tumor specific. This finding is of particular relevance to Neurofibromatosis, as *Nf1* haploinsufficient mast cells play important roles in the formation of neurofibromas due to their activation by SCF, the c-Kit ligand (9). There was no difference in the number of partially or fully degranulated mast cells between the two genotypes (Supplemental Figure 3). To further explore the link between elevated mast cell numbers and MPNSTs in $NI^{F/-}$ mice, we performed real time PCR for several cytokines involved in mast cell biology and recruitment. Indeed, levels of the mast cell-activating cytokine SCF were elevated in the tumors from $NI^{F/-}$ mice (Figure 4E), while levels of the mast cell-repressive cytokines CXCL1 and CXCL2 were decreased (41). Other cytokines whose role in mast cell biology are less well-defined were unchanged, including IL-10 and IL-6. Collectively, our results from flow cytometry and immunohistochemistry staining indicate that $CD11b^+$ $CD11c^-$ myeloid cells and mast cells are the two key hematopoietic cells enriched in the stroma of mouse $NI^{F/-}$ MPNSTs.

Mast cells are enriched in human NF1-associated MPNSTs

To examine the significance of the mast cell enrichment phenotype in human MPNST samples, we analyzed a tissue microarray of primary and locally recurrent MPNSTs with known NF1 status for c-Kit staining, a commonly used clinical marker of mast cells (31, 33). Mast cells were enriched in NF1-associated MPNSTs compared to sporadic MPNSTs (Figure 4F). Taken together, these data indicate that mast cells are enriched in human and mouse NF1-associated MPNSTs.

Influence of *Nf1* haploinsufficient stroma on response to chemotherapy

Chemotherapy can play an important role in treating advanced MPNST (42, 43), but overall survival remains low. Doxorubicin is the most common chemotherapy for advanced stage sarcoma (44), however response rates are low (17–27% for single-agent doxorubicin), and there are risks of significant cardiac toxicity associated with high cumulative doses of doxorubicin. In patients with NF1-associated sarcomas, the response rate may be even worse (14, 18). Improved outcomes may be found by optimizing chemotherapy regimens and combination treatments in clinical trials, but these studies are time-consuming and potentially expose patients to additional toxicity without benefit. There are conflicting reports as to the benefit of multi-agent chemotherapy for treating advanced MPNST in NF1 patients (42, 43). A clinical trial SARC006 (NCI-06-C-0043) attempted to determine if

MPNSTs from Neurofibromatosis patients would respond similarly as tumors from patients with wild-type *NF1* to a combined ifosfamide/doxorubicin regimen. Patients with NF1-associated MPNST and sporadic MPNST were enrolled and treated with doxorubicin and ifosfamide chemotherapy regimens (Figure 5A). Unfortunately, this clinical trial closed early due to poor accrual, and no clear differences in chemotherapy response were identified in this patient cohort (45). Therefore, we performed a trial in our primary mouse models to help define the role of the *Nf1* haploinsufficient tumor microenvironment in the therapeutic response to standard-of-care chemotherapies (Figure 5B). These mouse models are well-suited for preclinical studies, as the primary tumors develop within a native, immunocompetent tumor microenvironment and are spatially restricted, which facilitates accurate measurement of tumor volumes to assess treatment response. By defining the role of the tumor stroma in chemotherapy response in mouse models, we may inform the design of future clinical trials for Neurofibromatosis patients with MPNSTs.

Following injection of Ad-Cre into the sciatic nerve of $NI^{F/F}$ or $NI^{F/-}$ mice, MPNSTs of similar volume (200–300 mm^3) were treated with either vehicle alone or a single bolus of doxorubicin/ifosfamide (15 mg/kg i.p. Dox; 50 mg/kg IFO i.v.) (Figure 5B). Response to treatment was monitored by caliper measurement, and mice were sacrificed when tumor volume reached IACUC-approved endpoints. The majority of tumors treated with the Dox/IFO regime showed some initial tumor shrinkage and delay in tumor growth (Figure 5 C–D). MPNSTs from both $NI^{F/-}$ and $NI^{F/F}$ mice showed moderate partial response rate (50% vs. 45%, respectively, defined as >30% reduction in volume), and there was no difference in the size of tumors 10 days after treatment (1.20-fold vs. 1.15-fold change in size, p=0.95). Taken together, these data suggest that the status of *Nf1* in the surrounding stroma does not alter the growth response of MPNSTs to conventional chemotherapy.

Although there were no differences in tumor growth response between MPNSTs in $NI^{F/F}$ and $NI^{F/-}$ mice, we wondered if there could be differences in the molecular response to cytotoxic agents. Therefore, we analyzed vehicle-treated and Dox/IFO-responding MPNSTs for markers of cell proliferation (Ki67), apoptosis (cleaved Caspase 3), and mast cell infiltration (toluidine blue, Figure 5F and Supplemental Figure 4). In addition, we analyzed samples 48 hours after Dox/IFO treatment, as this time point has been reported to show maximum tumor cell death following doxorubicin exposure in mice (46). As expected, Ki67 levels were reduced in both genotypes at 48 hours, but were similar between vehicle-treated and responding tumors at terminal harvest. Cleaved caspase 3 levels were elevated at 48 hours post-Dox/IFO, suggesting cell death is increased directly following chemotherapy, but levels decrease by the time of terminal harvest. Importantly, there were no differences in cell death or proliferation markers between MPNSTs in $NI^{F/F}$ and $NI^{F/-}$ mice 48 hours post-Dox/IFO. This is similar to the tumor growth data in Figure 5C–D and supports the conclusion that these tumors respond similarly to Dox/IFO treatment, even at early time points. The number of mast cells was not altered by Dox/IFO treatment, and the enrichment of mast cells in $NI^{F/-}$ MPNSTs was still observed across all time points. This suggests that mast cells may not play a role in the response to conventional chemotherapy, which could explain why there is no difference in response between the two genotypes. Taken together, these data using primary mouse models show that MPNSTs in mice respond similarly to a combination treatment with doxorubicin and ifosfamide, irrespective of stromal genotype.

Discussion

Although NF1-associated MPNSTs are surrounded by a tumor microenvironment of *NF1* haploinsufficient cells, it is unknown if elevated NF1-dependent signaling in these stromal cells influences MPSNT biology. Both anecdotal reports and clinical studies have suggested that NF1-associated MPNSTs have a worse outcome than sporadic MPSNTs, but to our knowledge this has never been addressed in an experimental model, nor has there been any mechanistic explorations of potential biological differences. Here, we used paired littermate mice to model the distinct genetics of the tumor microenvironment in NF1-associated and sporadic MPSNTs. $NI^{F/-}$ mice, which model *Nf1* haploinsufficiency, developed MPNSTs at an accelerated rate with an elevated immune cell infiltrate that was characterized by increased numbers of $CD11b^{+}CD11c^{-}$ myeloid cells and mast cells. Analysis of patient samples showed that MPNSTs in NF1 patients are also enriched for the presence of mast cells. Moreover, the *Nf1* haploinsufficient hematopoietic compartment was sufficient to accelerate tumor development, further underscoring the importance of the immune system in modifying MPNST biology. While it is possible that Adeno-Cre injection into the nerve of $NI^{F/-}$ mice may not only delete *Nf1* and *Ink4a/Arf* in Schwann cells, but may also delete these tumor suppressors from surrounding stromal cells, the bone marrow transplant experiment indicates that deletion of *Nf1* and *Ink4a/Arf* in stromal cells does not contribute to the accelerated formation of MPNST in these mice. Instead, the bone marrow transplant experiment demonstrates a fundamental role for the *Nf1* +/− hematopoietic compartment, which is independent of any effect of Adenoviral infection of stromal cells.

Given the hyperactive Ras signaling that has been reported in several NF1-deficient cells—including endothelial cells, fibroblasts, and immune cells—we initially hypothesized that the number of these cell types would be altered in $NI^{F/-}$ tumors. The *Nf1* haploinsufficient stroma plays a well-known role in the etiology of the Neurofibromatosis disease spectrum. *Nf1* +/− endothelial cells are hyper-responsive to VEGF signaling, which results in neovascularization and altered vascular morphogenesis (47). Fibroblasts haploinsufficient for neurofibromin proliferate at accelerated rates and secrete excess levels of collagen (48). NF1-associated myeloid cells, including mast cells and macrophages, are involved in neurofibroma development and resistance to targeted therapies, respectively (9, 49). However, the role of these cells in the MPNST tumor microenvironment has not been previously explored.

Given the many cell types and functions that are altered by *Nf1* loss, we were surprised that only levels of CD45+ immune cells were altered in $NI^{F/-}$ MPNSTs. Initially, we suspected macrophages were the key immune cell population altered in $NI^{F/-}$ tumors, as multiple studies have shown a key role for macrophages in NF1 disease biology, but immunohistochemistry showed no difference in macrophage markers. Instead, we found that the increased $CD45^{+}$ population was comprised primarily of $CD11b^{+}$ $CD11c^{-}$ myeloid cells and mast cells. Further experiments, such as using lineage-specific cell depletion (50), are required to determine if monocytes, mast cells, or other cell types, are necessary for accelerating formation of $NI^{F/-}$ MPNSTs. Indeed, a combination of signaling networks in these cell types may be necessary to optimally accelerate tumor formation by the *Nf1* haploinsufficient hematopoietic compartment. Several hypotheses for how these cells may

alter tumor initiation include influencing angiogenesis or producing a cytokine storm that alters immune cell signaling at early time points.

Mast cells have long been recognized as important contributors to Neurofibromatosis disease phenotypes, and *in vitro* studies have shown that *Nf1* haploinsufficient mast cells are hyper-responsive to SCF in the neurofibroma environment. Activated mast cells secrete elevated cytokines, which may accelerate MPNST formation. Mast cells are enriched in NF1-associated neurofibromas and MPNSTs when compared to control skin and nerve (51). Of note, the first clinical trial for neurofibromas in Neurofibromatosis patients aimed to limit mast cell numbers via ketotifen administration (7, 52). Experiments in mice showed that neurofibroma formation was influenced by cKit-positive cells in the stroma (9), although it is important to note that the cKit-knockout model is not exclusive to mast cells (53, 54). Treatment of several patients with imatinib, a Kit inhibitor, decreased the growth of head and neck neurofibromas, however less efficacy was observed for neurofibromas at other locations (55). Taken together, these data support a central role of the mast cell in NF1 biology. Future studies will determine the contribution and mechanism of mast cells and/or monocytes to the *Nf1* haploinsufficient tumor microenvironment and MPNST biology.

Generating sarcomas in a temporally-restricted manner at a spatially restricted site facilitates measuring tumor volumes and allows accurate assessment of treatment response. Because the primary tumors develop within a native, immunocompetent, tumor microenvironment, we were able to model the effects of an *Nf1* haploinsufficient immune system on conventional chemotherapy. In the future, we will be able to use these models to study the impact of an *Nf1* haploinsufficient immune system on immunotherapy. The spatially-restricted nature of this model also facilitates the analysis of changes in tumor histology at distinct points following chemotherapy treatment. This analysis allowed us to examine changes in proliferation and cell death within the tumor across different time points after treatment. Our data shows that MPNSTs in $NI^{F/F}$ and $NI^{F/-}$ mice respond similarly to conventional chemotherapy, helping to clarify the impact of *Nf1* haploinsufficient stroma on tumor response to multi-agent chemotherapy. Thus, our results may inform future clinical trials because they suggest that the NF1-associated and sporadic MPNSTs can be grouped together in study arms for conventional chemotherapy. Although *Nf1* haploinsufficient stroma did not impact response to chemotherapy in our mouse models, our finding of a differential immune environment between NF1-associated and sporadic MPNSTs suggest that response to immunotherapy or other targeted therapies may be impacted by *NF1* haploinsufficiency. Future studies using these and other models will help clarify the impact of the distinct NF1-assoicated immune microenvironment on these therapies.

Supplementary Material

Refer to Web version on PubMed Central for supplementary material.

Acknowledgments

We thank Ron Dephino for providing the $Ink4a/Arf^{Flox/Flox}$ mice. We thank Rich Riedel for helpful suggestions regarding the chemotherapy regimen for the co-clinical trial and members of the Kirsch lab for useful discussion and suggestions. This work was supported by W81XWH-14-1-0067 grant from the Department of Defense (DGK).

References

1. Serrano C, R C, Hernández-Losa J, Simonetti S, Valverde C, Moliné T, Somoza R, Pérez M, Vélez R, Vergés R, Domínguez R, Carles J, Ramón Y, Cajal S. RAS/MAPK pathway hyperactivation determines poor prognosis in undifferentiated pleomorphic sarcomas. Cancer. 2016; 22:99–107.
2. Dodd R. Emerging targets in sarcoma: Rising to the challenge of RAS signaling in undifferentiated pleomorphic sarcoma. Cancer. 2016; 22:17–19.
3. Eisinger-Mathason TS1, Z M, Qiu Q, Skuli N, Nakazawa MS, Karakasheva T, Mucaj V, Shay JE, Stangenberg L, Sadri N, Puré E, Yoon SS, Kirsch DG, Simon MC. Hypoxia-dependent modification of collagen networks promotes sarcoma metastasis. Cancer discovery. 2013; 3:1190–1205. [PubMed: 23906982]
4. Chen X, Stewart E, Shelat AA, Qu C, Bahrami A, Hatley M, Wu G, Bradley C, McEvoy J, Pappo A, Spunt S, Valentine MB, Valentine V, Krafcik F, Lang WH, Wierdl M, Tsurkan L, Tolleman V, Federico SM, Morton C, Lu C, Ding L, Easton J, Rusch M, Nagahawatte P, Wang J, Parker M, Wei L, Hedlund E, Finkelstein D, Edmonson M, Shurtleff S, Boggs K, Mulder H, Yergeau D, Skapek S, Hawkins DS, Ramirez N, Potter PM, Sandoval JA, Davidoff AM, Mardis ER, Wilson RK, Zhang J, Downing JR, Dyer MA. St. Jude Children's Research Hospital-Washington University Pediatric Cancer Genome, P. Targeting oxidative stress in embryonal rhabdomyosarcoma. Cancer cell. 2013; 24:710–724. [PubMed: 24332040]
5. Shern JF, Chen L, Chmielecki J, Wei JS, Patidar R, Rosenberg M, Ambrogio L, Auclair D, Wang J, Song YK, Tolman C, Hurd L, Liao H, Zhang S, Bogen D, Brohl AS, Sindiri S, Catchpoole D, Badgett T, Getz G, Mora J, Anderson JR, Skapek SX, Barr FG, Meyerson M, Hawkins DS, Khan J. Comprehensive genomic analysis of rhabdomyosarcoma reveals a landscape of alterations affecting a common genetic axis in fusion-positive and fusion-negative tumors. Cancer discovery. 2014; 4:216–231. [PubMed: 24436047]
6. Barretina J, Taylor BS, Banerji S, Ramos AH, Lagos-Quintana M, Decarolis PL, Shah K, Socci ND, Weir BA, Ho A, Chiang DY, Reva B, Mermel CH, Getz G, Antipin Y, Beroukhim R, Major JE, Hatton C, Nicoletti R, Hanna M, Sharpe T, Fennell TJ, Cibulskis K, Onofrio RC, Saito T, Shukla N, Lau C, Nelander S, Silver SJ, Sougnez C, Viale A, Winckler W, Maki RG, Garraway LA, Lash A, Greulich H, Root DE, Sellers WR, Schwartz GK, Antonescu CR, Lander ES, Varmus HE, Ladanyi M, Sander C, Meyerson M, Singer S. Subtype-specific genomic alterations define new targets for soft-tissue sarcoma therapy. Nature genetics. 2010; 42:715–721. [PubMed: 20601955]
7. Ratner N, M S. RASopathy gene commonly mutated in cancer: the neurofibromatosis type 1 tumour suppressor. Nat. Rev. Cancer. 5
8. Staser K, Yang FC, Clapp DW. Mast cells and the neurofibroma microenvironment. Blood. 116:157–164.
9. Yang FC, Ingram DA, Chen S, Zhu Y, Yuan J, Li X, Yang X, Knowles S, Horn W, Li Y, Zhang S, Yang Y, Vakili ST, Yu M, Burns D, Robertson K, Hutchins G, Parada LF, Clapp DW. Nf1-dependent tumors require a microenvironment containing Nfl/− and c-kit-dependent bone marrow. Cell. 2008; 135:437–448. [PubMed: 18984156]
10. Wu J, Williams JP, Rizvi TA, Kordich JJ, Witte D, Meijer D, Stemmer-Rachamimov AO, Cancelas JA, Ratner N. Plexiform and dermal neurofibromas and pigmentation are caused by Nf1 loss in desert hedgehog-expressing cells. Cancer cell. 2008; 13:105–116. [PubMed: 18242511]
11. Le LQ, S T, Burns DK, Parada LF. Cell of origin and microenvironment contribution for NF1-associated dermal neurofibromas. Cell stem cell. 2009; 4:453–463. [PubMed: 19427294]
12. BC W. Current status of sporadic and neurofibromatosis type 1-associated malignant peripheral nerve sheath tumors. Curr Oncol Rep. 2009; 11
13. Zou C, Smith KD, Liu J, Lahat G, Myers S, Wang WL, Zhang W, McCutcheon IE, Slopis JM, Lazar AJ, Pollock RE, Lev D. Clinical, pathological, and molecular variables predictive of malignant peripheral nerve sheath tumor outcome. Annals of surgery. 2009; 249:1014–1022. [PubMed: 19474676]
14. Evans DG, Baser ME, McGaughran J, Sharif S, Howard E, Moran A. Malignant peripheral nerve sheath tumours in neurofibromatosis 1. Journal of medical genetics. 2002; 39:311–314. [PubMed: 12011145]

15. Zhou H, C C, Perkins SL, Tripp SR, Liew M, Viskochil DH, et al. Malignant peripheral nerve sheath tumor: a comparison of grade, immunophenotype, and cell cycle/growth activation marker expression in sporadic and neurofibromatosis 1-related lesions. The American journal of surgical pathology. 2003; 27:1337–1345. [PubMed: 14508395]
16. Zehou O, F E, Zelek L, Sbidian E, Ortonne N, Banu E, Wolkenstein P, Valeyrie-Allanore L. Chemotherapy for the treatment of malignant peripheral nerve sheath tumors in neurofibromatosis 1: a 10-year institutional review. Orphanet J Rare Dis. 2013; 23
17. Kolberg M, Høland M, Ågesen TH, Brekke HR, Liestøl K, Hall KS, Mertens F, Picci P, Smeland S, Lothe RA. Survival meta-analyses for >1800 malignant peripheral nerve sheath tumor patients with and without neurofibromatosis type 1. Neuro-Oncology. 2013; 15:135–147. [PubMed: 23161774]
18. Ferrari A, Miceli R, Rey A, Oberlin O, Orbach D, Brennan B, Mariani L, Carli M, Bisogno G, Cecchetto G, De Salvo GL, Casanova M, Vannoesel MM, Kelsey A, Stevens MC, Devidas M, Pappo AS, Spunt SL. Non-metastatic unresected paediatric non-rhabdomyosarcoma soft tissue sarcomas: results of a pooled analysis from United States and European groups. Eur J Cancer. 47:724–731.
19. Watson KL, AS G, Kivlin CM, Ingram DR, Landers SM, Roland CL, Cormier JN, Hunt KK, Feig BW, Ashleigh Guadagnolo B, Bishop AJ, Wang WL, Slopis JM, McCutcheon IE, Lazar AJ, Torres KE. Patterns of recurrence and survival in sporadic, neurofibromatosis Type 1-associated, and radiation-associated malignant peripheral nerve sheath tumors. J. Neurosurg. 2016; 1:1–11.
20. Dodd RD, Mito JK, Eward WC, Chitalia R, Sachdeva M, Ma Y, Barretina J, Dodd L, Kirsch DG. NF1 deletion generates multiple subtypes of soft-tissue sarcoma that respond to MEK inhibition. Molecular cancer therapeutics. 2013; 12:1906–1917. [PubMed: 23858101]
21. Perrone F, Tabano S, Colombo F, Dagrada G, Birindelli S, Gronchi A, Colecchia M, Pierotti MA, Pilotti S. p15INK4b, p14ARF, and p16INK4a inactivation in sporadic and neurofibromatosis type 1-related malignant peripheral nerve sheath tumors. Clinical Cancer Research. 2003; 9:4132–4138. [PubMed: 14519636]
22. Lee W, T S, Wiesner T, Ran L, Prieto Granada CN, Lin M, Zhu S, Cao Z, Liang Y, Sboner A, Tap WD, Fletcher JA, Huberman KH, Qin LX, Viale A, Singer S, Zheng D, Berger MF, Chen Y, Antonescu CR, Chi P. PRC2 is recurrently inactivated through EED or SUZ12 loss in malignant peripheral nerve sheath tumors. Nature genetics. 2014; 46:1227–1232. [PubMed: 25240281]
23. Zhu Y, Romero MI, Ghosh P, Ye Z, Charnay P, Rushing EJ, Marth JD, Parada LF. Ablation of NF1 function in neurons induces abnormal development of cerebral cortex and reactive gliosis in the brain. Genes & development. 2001; 15:859–876. [PubMed: 11297510]
24. Jacks T, Shih TS, Schmitt EM, Bronson RT, Bernards A, Weinberg RA. Tumour predisposition in mice heterozygous for a targeted mutation in Nf1. Nature genetics. 1994; 7:353–361. [PubMed: 7920653]
25. Aguirre AJ, Bardeesy N, Sinha M, Lopez L, Tuveson DA, Horner J, Redston MS, DePinho RA. Activated Kras and Ink4a/Arf deficiency cooperate to produce metastatic pancreatic ductal adenocarcinoma. Genes & development. 2003; 17:3112–3126. [PubMed: 14681207]
26. Dodd RD AL, Blum JM, Li Z, Van Mater D, Kirsch DG. Methods to generate genetically engineered mouse models of soft tissue sarcoma. Methods Mol Biol. 2015; 1267:283–295. [PubMed: 25636474]
27. Dodd RD, Sachdeva M, Mito JK, Eward WC, Brigman BE, Ma Y, Dodd L, Kim Y, Lev D, Kirsch DG. Myogenic transcription factors regulate pro-metastatic miR-182. Oncogene. 2016; 35:1868–1875. [PubMed: 26234681]
28. Lee CL, C K, Moding EJ, Blum JM, Williams N, Luo L, Ma Y, Borst LB, Kim Y, Kirsch DG. Acute DNA damage activates the tumour suppressor p53 to promote radiation-induced lymphoma. Nat Commun. 2015; 24:8477.
29. Sachdeva M, M J, Lee C, Zhang M, Li Z, Dodd R, Cason D, Luo L, Ma Y, Vanmater D, Gladdy R, Lev D, Cardona D, Kirsch D. MicroRNA-182 drives metastasis of primary sarcomas by targeting multiple genes. Journal of Clincal Investigations. 2014; 124:4305–4319.
30. Youn J-I, Nagaraj S, Collazo M, Gabrilovich DI. Subsets of Myeloid-Derived Suppressor Cells in Tumor Bearing Mice. Journal of immunology (Baltimore, Md. : 1950). 2008; 181:5791–5802.

31. Cleven AH, S G, Briaire-de Bruijn I, Ingram DR, van de Rijn M, Rubin BP, de Vries MW, Watson KL, Torres KE, Wang WL, van Duinen SG, Hogendoorn PC, Lazar AJ, Bovée JV. Loss of H3K27 trimethylation is a diagnostic marker for malignant peripheral nerve sheath tumors and an indicator for an inferior survival. Mod Pathol. 2016; 29:582–590. [PubMed: 26990975]
32. Torres-Cabala CA, W W, Trent J, Yang D, Chen S, Galbincea J, Kim KB, Woodman S, Davies M, Plaza JA, Nash JW, Prieto VG, Lazar AJ, Ivan D. Correlation between KIT expression and KIT mutation in melanoma: a study of 173 cases with emphasis on the acral-lentiginous/mucosal type. Mod Pathol. 2009; 22:1446–1456. [PubMed: 19718013]
33. Zou C, S K, Liu J, Lahat G, Myers S, Wang WL, Zhang W, McCutcheon IE, Slopis JM, Lazar AJ, Pollock RE, Lev D. Clinical, pathological, and molecular variables predictive of malignant peripheral nerve sheath tumor outcome. Annals of surgery. 2009; 249:1014–1022. [PubMed: 19474676]
34. Kim S, D R, Mito JK, Ma Y, Kim Y, Riedel RF, Kirsch DG. Efficacy of phosphatidylinositol-3 kinase (PI3K) inhibitors in a primary mouse model of undifferentiated pleomorphic sarcoma (UPS). Sarcoma. 2012
35. Staser K, Yang F-C, Clapp DW. Pathogenesis of Plexiform Neurofibroma: Tumor-Stromal/ Hematopoietic Interactions in Tumor Progression. Annual review of pathology. 2012; 7:469–495.
36. Beacham DA, C E. Stromagenesis: the changing face of fibroblastic microenvironments during tumor progression. Seminars in cancer biology. 2005; 15:329–341. [PubMed: 15970443]
37. Chlenski A, G L, Yang Q, Tian Y, Peddinti R, Salwen HR, Cohn SL. SPARC enhances tumor stroma formation and prevents fibroblast activation. Oncogene. 2007; 5:4513–4522.
38. Welte T, K I, Tian L, Gao X, Wang H, Li J, Holdman XB, Herschkowitz JI, Pond A, Xie G, Kurley S, Nguyen T, Liao L, Dobrolecki LE, Pang L, Mo Q, Edwards DP, Huang S, Xin L, Xu J, Li Y, Lewis MT, Wang T, Westbrook TF, Rosen JM, Zhang XH. Oncogenic mTOR signalling recruits myeloid-derived suppressor cells to promote tumour initiation. Nat Cell Biol. 2016; 18:632–644. [PubMed: 27183469]
39. Wang DJ, R N, Byrd JC, Guttridge DC. NF-κB functions in tumor initiation by suppressing the surveillance of both innate and adaptive immune cells. Cell Reports. 2014; 9:90–103. [PubMed: 25263557]
40. Wernersson S, P G. Mast cell secretory granules: armed for battle. Nat Rev Immunol. 2014; 14:478–494. [PubMed: 24903914]
41. khouri H, M L, Armour CL, Hughes JM. CXCL1 is a negative regulator of mast cell chemotaxis to airway smooth muscle cell products in vitro. Clin Exp Allergy. 2014; 44:381–392. [PubMed: 24588865]
42. Kroep JR, Ouali M, Gelderblom H, Le Cesne A, Dekker TJ, Van Glabbeke M, Hogendoorn PC, Hohenberger P. First-line chemotherapy for malignant peripheral nerve sheath tumor (MPNST) versus other histological soft tissue sarcoma subtypes and as a prognostic factor for MPNST: an EORTC soft tissue and bone sarcoma group study. Ann Oncol. 2011; 22:207–214. [PubMed: 20656792]
43. Moretti VM, Crawford EA, Staddon AP, Lackman RD, Ogilvie CM. Early outcomes for malignant peripheral nerve sheath tumor treated with chemotherapy. American journal of clinical oncology. 34:417–421.
44. Lorigan P, Verweij J, Papai Z, Rodenhuis S, Le Cesne A, Leahy MG, Radford JA, Van Glabbeke MM, Kirkpatrick A, Hogendoorn PC, Blay JY. Phase III trial of two investigational schedules of ifosfamide compared with standard-dose doxorubicin in advanced or metastatic soft tissue sarcoma: a European Organisation for Research and Treatment of Cancer Soft Tissue and Bone Sarcoma Group Study. J. Clin. Oncol. 2007; 25:3144–3150. [PubMed: 17634494]
45. Widemann BC, R D, Helman LJ, Ludwig JA, Schuetze S, Staddon A, Milhem M, Rushing DA, Moertel CL, Goldman S, Livingston M, LWagner LM, Rodler ET, Dombi E, Perry A, Annunziata CM, Long L, Viskochil D, Steinberg SM, Baker LH. SARC006: Phase II trial of chemotherapy in sporadic and neurofibromatosis type 1 (NF1)-associated high-grade malignant peripheral nerve sheath tumors (MPNSTs). J Clin Oncol. 2013; 31 2013 (suppl; abstr 10522).
46. MacKay JA, C M, McDaniel JR, Liu W, Simnick AJ, Chilkoti A. Self-assembling chimeric polypeptide-doxorubicin conjugate nanoparticles that abolish tumours after a single injection. Nat Mater. 2009; 8:993–999. [PubMed: 19898461]

47. Wu M, W M, Muir D. Nf1 haploinsufficiency augments angiogenesis. Oncogene. 2006; 25:2297–2303. [PubMed: 16288202]

48. Atit RP, C M, Greenhalgh DG, Wenstrup RJ, Ratner N. The Nf1 tumor suppressor regulates mouse skin wound healing, fibroblast proliferation, and collagen deposited by fibroblasts. J Invest Dermatol. 1999; 112:835–842. [PubMed: 10383727]

49. Prada CE, J E, Rizvi TA, Wu J, Dunn RS, Mayes DA, Cancelas JA, Dombi E, Kim MO, West BL, Bollag G, Ratner N. Neurofibroma-associated macrophages play roles in tumor growth and response to pharmacological inhibition. Acta Neuropathol. 2013; 125:159–168. [PubMed: 23099891]

50. Schönhuber N, S B, Schuck K, Veltkamp C, Schachtler C, Zukowska M, Eser S, Feyerabend TB, Paul MC, Eser P, Klein S, Lowy AM, Banerjee R, Yang F, Lee CL, Moding EJ, Kirsch DG, Scheideler A, Alessi DR, Varela I, Bradley A, Kind A, Schnieke AE, Rodewald HR, Rad R, Schmid RM, Schneider G, Saur D. A next-generation dual-recombinase system for time- and host-specific targeting of pancreatic cancer. Nature medicine. 2014; 20:1340–1347.

51. Friedrich RE, N U, Glatzel M, Hagel C. Vessel and Mast Cell Densities in Sporadic and Syndrome-associated Peripheral Nerve Sheath Tumors. Anticancer research. 2015; 35:4713–4722. [PubMed: 26254361]

52. Riccardi V. Current Utilization of Mast Cell Stabilizers for Preemptive Treatments of NF1 Neurofibromas. Neuro Open J. 2015; 2:67–73.

53. Gomez-Pinilla PJ, F G, Di Giovangiulio M, Stakenborg N, Némethova A, de Vries A, Liston A, Feyerabend TB, Rodewald HR, Boeckxstaens GE, Matteoli G. Mast cells play no role in the pathogenesis of postoperative ileus induced by intestinal manipulation. PloS one. 2014; 9:e85304. [PubMed: 24416383]

54. Reber LL, M T, Galli SJ. New models for analyzing mast cell functions in vivo. Trends Immunol. 2012; 33:613–625. [PubMed: 23127755]

55. Robertson KA, N G, Yang FC, Bowers DC, Ho CY, Hutchins GD, Croop JM, Vik TA, Denne SC, Parada LF, Hingtgen CM, Walsh LE, Yu M, Pradhan KR, Edwards-Brown MK, Cohen MD, Fletcher JW, Travers JB, Staser KW, Lee MW, Sherman MR, Davis CJ, Miller LC, Ingram DA, Clapp DW. Imatinib mesylate for plexiform neurofibromas in patients with neurofibromatosis type 1: a phase 2 trial. Lancet Oncol. 2012; 13:1218–1224. [PubMed: 23099009]

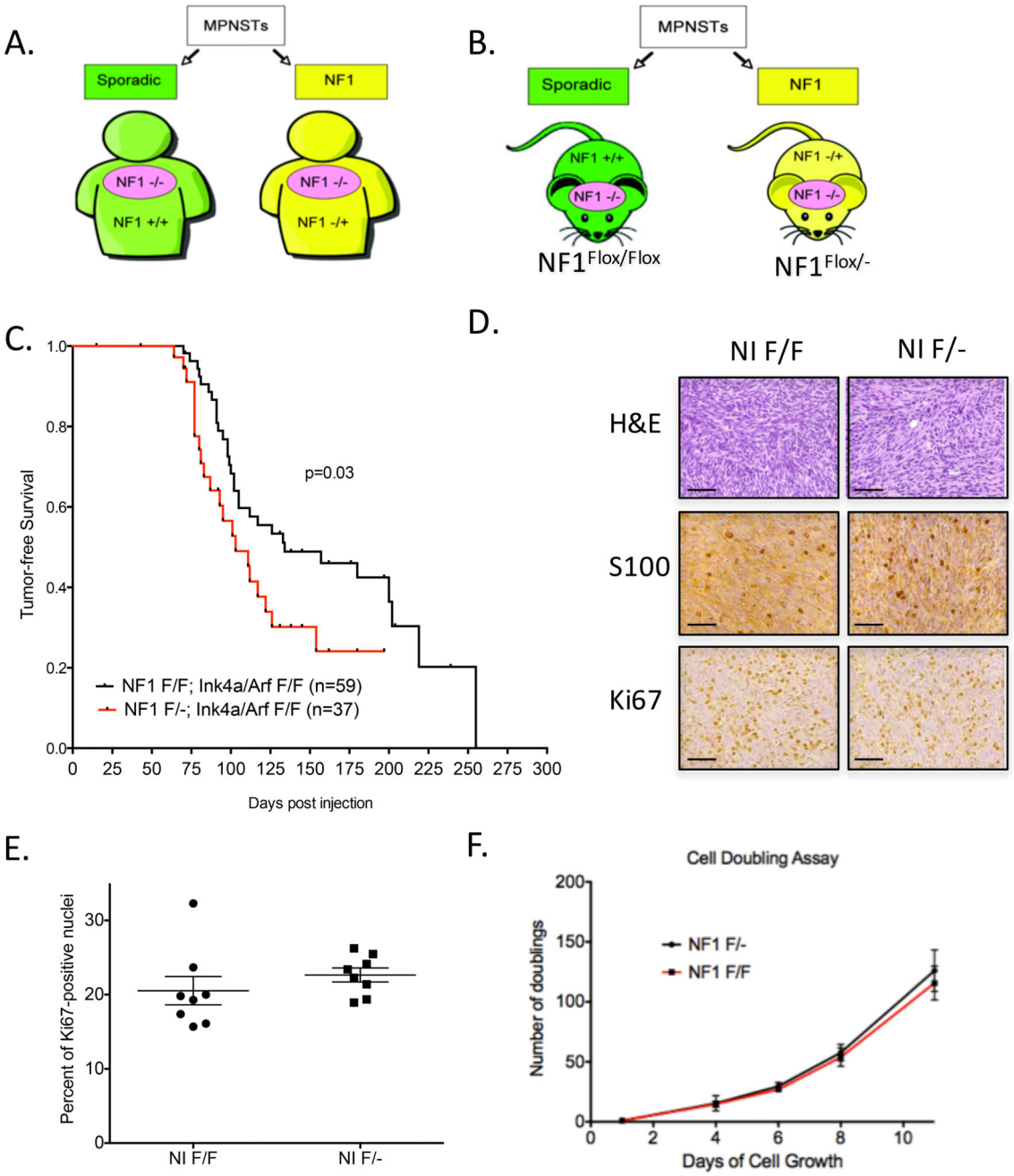

Figure 1. ***Nf1*** **haploinsufficient stroma accelerates MPNST development**

(A) MPNSTs (pink ovals) develop in two distinct genetic contexts: Sporadic MPNSTs (green) have stroma with wild-type *Nf1* (*Nf1* +/+), while NF1-assoicated MPNSTs (yellow) have *Nf1* haploinsufficient stroma (*Nf1* +/−). (B) Paired littermate mice were designed to replicate the genetics of sporadic (green; $NI^{F/F}$ mice) and NF1-associated (yellow; $NI^{F/-}$ mice) MPNSTs. (C) MPNSTs generated in $NI^{F/-}$ mice develop MPNSTs at an accelerated rate. (D) Histological examination shows MPNSTs in $NI^{F/F}$ and $NI^{F/-}$ mice are indistinguishable by cell morphology, S100 staining, and Ki67 levels. E) Ki67 index is similar between MPNSTs in $NI^{F/F}$ and $NI^{F/-}$ mice. (F) Cells from $NI^{F/F}$ and $NI^{F/-}$ MPNSTs

proliferate at similar rates in vitro. Data shown are averages of three independent cell lines of each genotype. Scale bar is equal to 100 microns.

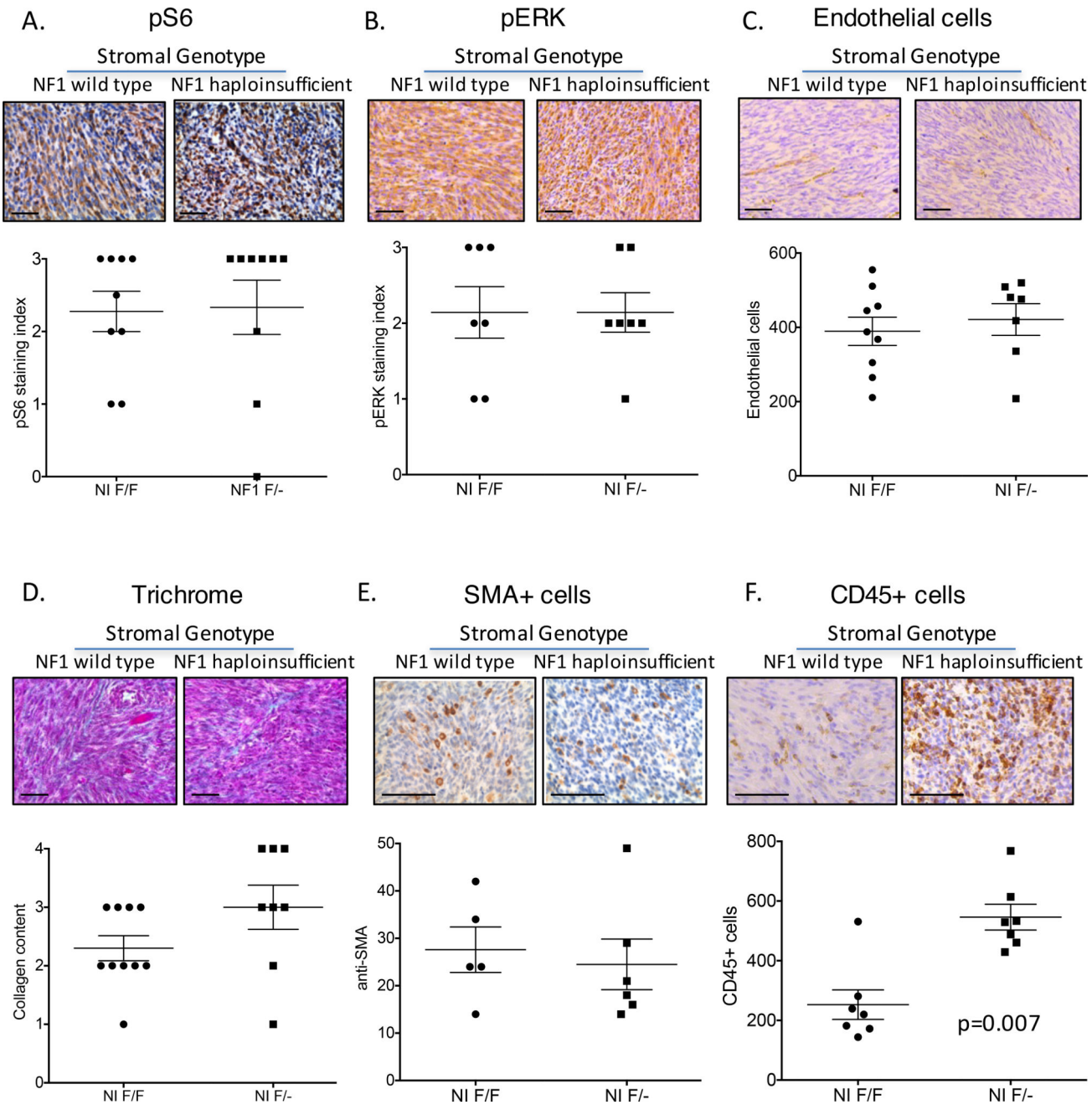

Figure 2. The *Nf1* haploinsufficient microenvironment alters CD45+ immune cell infiltration into MPNSTs

MPNSTs from $NI^{F/F}$ and $NI^{F/-}$ mice were examined for cell signaling molecules (A–B) and stromal cell components. No difference was found between the two genotypes of mice for pS6 levels (A), pERK levels (B), endothelial cell content measured by CD31+ (C), fibroblast activity, measured by collagen production via Masson's Trichrome (D), or fibroblast number, measured by SMA staining (E). (F) CD45+ immune cells were enriched in MPNSTs in $NI^{F/-}$ mice. Each point represents a single tumor that was analyzed by 6 independent fields of slide. Scale bar is equal to 100 microns.

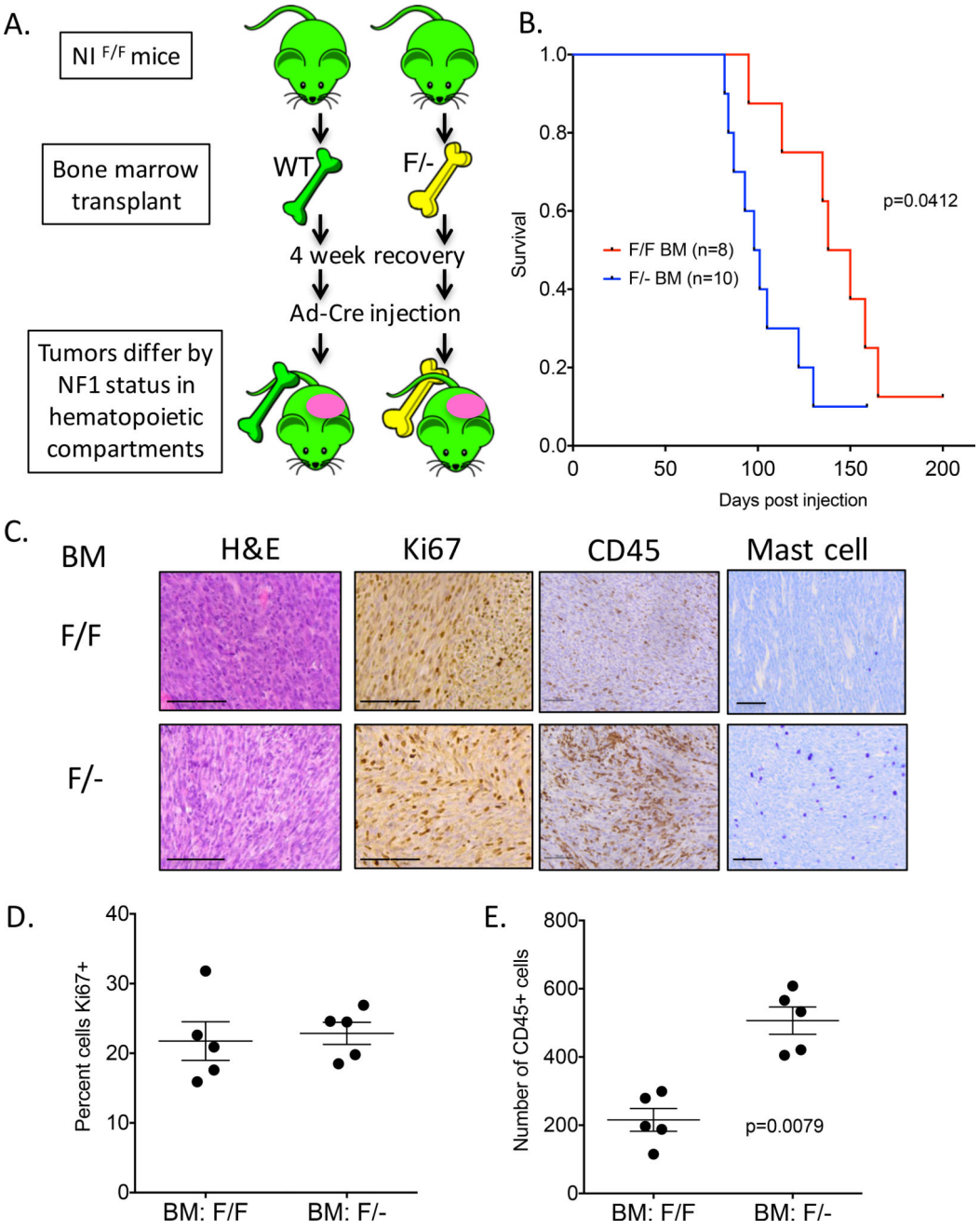

Figure 3. The *Nf1* haploinsufficient bone marrow compartment is sufficient to accelerate MPNST formation

(A) Schematic of bone marrow transplant. Recipient mice were all $NI^{F/F}$ and received either $NI^{F/F}$ or $NI^{F/-}$ bone marrow containing a fluorescent reporter. After 4 weeks of recovery, the mice were injected with Ad-Cre into the sciatic nerve and monitored for MPNST development. (B). Mice that received $NI^{F/-}$ bone marrow developed MPNST earlier than mice that received $NI^{F/F}$ bone marrow. (C–E) MPNSTs from mice that received $NI^{F/-}$ bone marrow showed similar levels of Ki67 staining as mice that received $NI^{F/F}$ bone marrow, but $NI^{F/-}$ MPNSTs were enriched in CD45+ cells. Scale bar is equal to 100 microns.

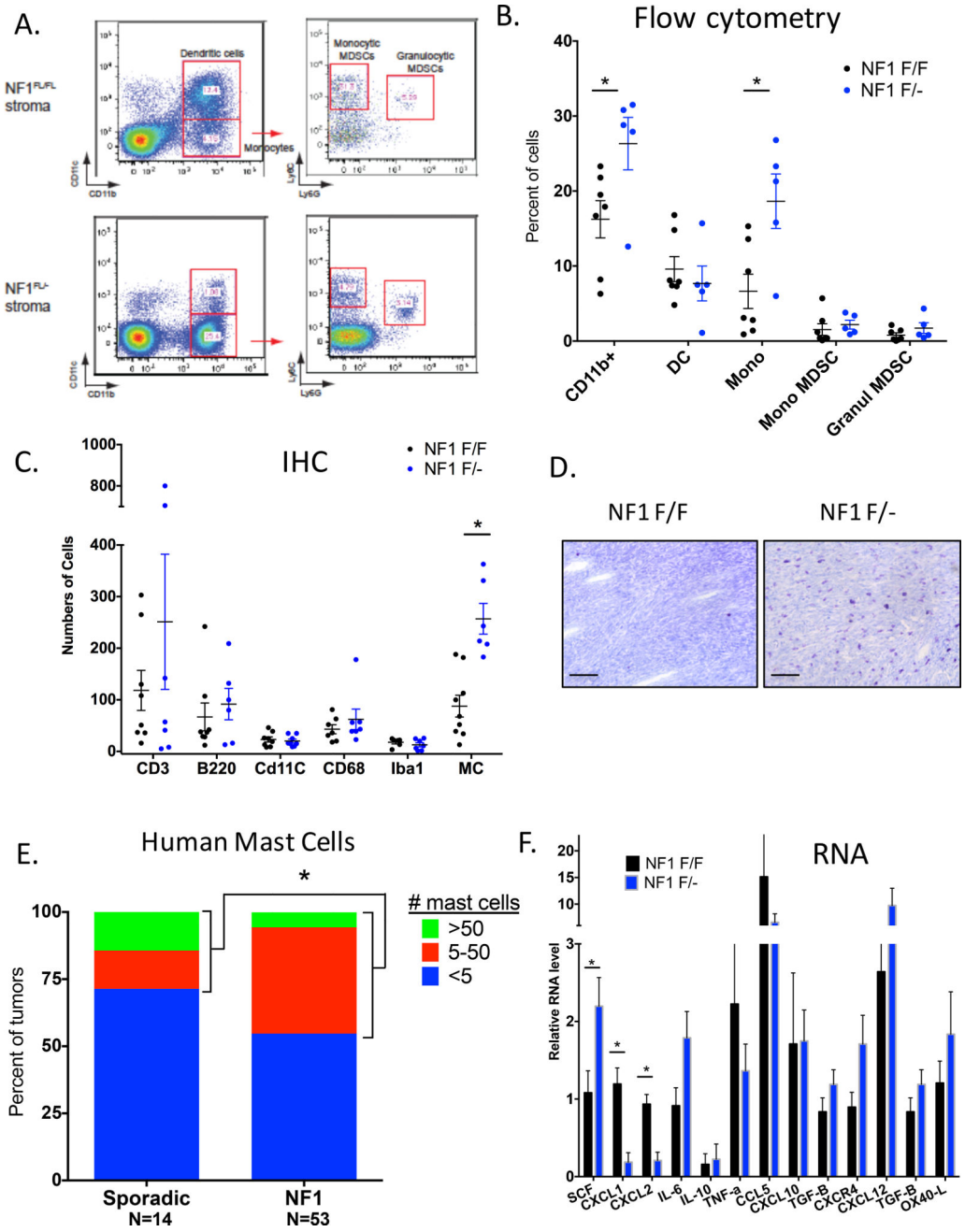

Figure 4. The immune cell infiltrate in *Nf1* haploinsufficient MPNSTs is enriched for CD11b $^{+}$CD11c^{-} myeloid cells and mast cells

(A) Flow cytometry schematic to analyze immune cell population in NI$^{F/F}$ and NI$^{F/-}$ MPNSTs. The percentage of CD11b^{+}CD11c^{-} monocytes is greatly increased in the NI$^{F/-}$ tumors. (B) Quantification of flow cytometry analyses for the percentage of CD11b^{+} cells, CD11b^{+}CD11c^{+}dendritic cells, CD11b^{+}CD11c^{-} monocytes (Mono), monocytic myeloid derived suppresser cells (MDSCs) (CD11b^{+} CD11c^{-} Ly6G^{-} Ly6C^{high}), and granulocytic MDSCs (CD11b^{+} CD11c^{-} Ly6G^{+} Ly6C^{low}) in single cells dissociated from the whole tumor. Five tumors were analyzed per genotype. (C) Quantification of immunohistochemical analysis of MPNST samples examining levels of T cells (CD3), B cells (B220), dendritic

cells (CD11C), macrophages (CD68 and Iba1) and mast cells (toluidine blue). Only mast cells were enriched in $NI^{F/-}$ tumors. (D) Toludine blue stained MPNSTs demonstrating mast cell enrichment in $NI^{F/-}$ tumors. Scale bar is equal to 100 microns. (E) Quantification of KIT+ mast cells in tissue microarrays of 67 human MPNSTs showing mast cells are enriched in NF1-associated MPNSTs. (F) Real time PCR of mouse MPNSTs examining expression of genes involved in mast cell recruitment. Note elevated levels of SCF, the cKit ligand. Values are an average of 5 independent tumors per genotype with SEM.

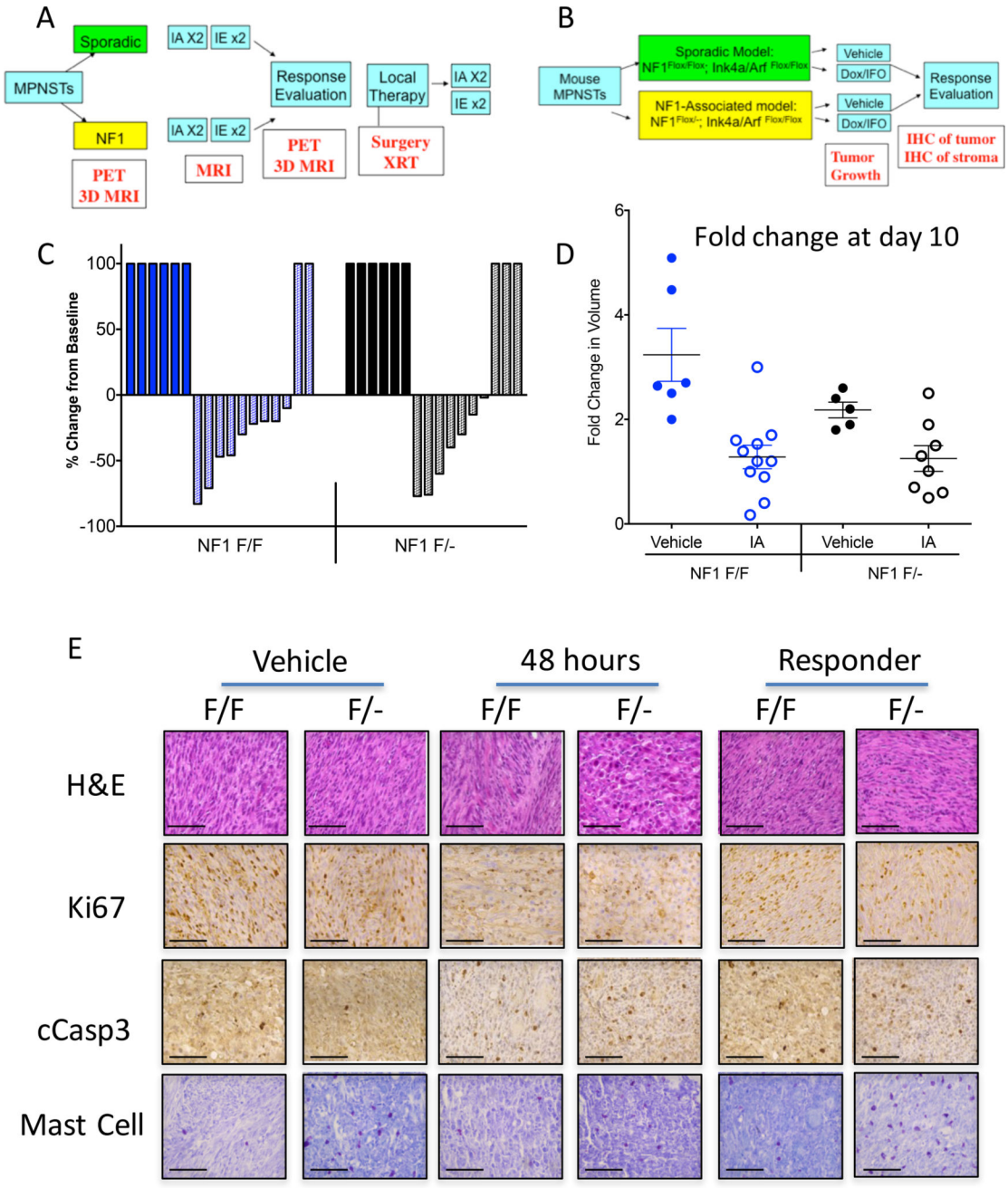

Figure 5. The *Nf1* haploinsufficient tumor microenvironment does not alter the response to conventional chemotherapy

(A) Schematic of SARC006 clinical trial design to compare response to doxorubicin/ifosfamide chemotherapy between sporadic and NF1-associated MPNSTs in human patients. (B) Schematic of mouse preclinical trial to compare response to doxorubicin/ifosfamide chemotherapy between MPNSTs in $NI^{F/F}$ and $NI^{F/-}$ mice. (C) Waterfall plot of mouse MPNSTs treated with vehicle alone (solid bars) or doxorubicin/ifosfamide combination (shaded bars). There was no difference in response rates between $NI^{F/F}$ and $NI^{F/-}$ mice. (D) Fold change in initial tumor volume 10 days after dose of doxorubicin/ifosfamide. Both $NI^{F/F}$ and $NI^{F/-}$ MPNSTs showed similar changes in volume following treatment. (E)

Histology of mouse MPNSTs treated with vehicle alone, 48 hours after doxorubicin/ifosfamide treatment, or after terminal harvest from responding to doxorubicin/ifosfamide treatment. Ki67 levels were decreased 48 hours after treatment, whereas cleaved caspase 3 levels were elevated 48 hours post-treatment. There were no differences between $NI^{F/F}$ and $NI^{F/-}$ mice following chemotherapy at either 48 hours or at terminal harvest. Mast cell numbers remained elevated in $NI^{F/-}$ MPNSTs throughout the experiment. Scale bar is equal to 100 microns.